Allowed and forbidden transitions in artificial hydrogen and helium atoms

Toshimasa Fujisawa*, David Guy Austing*†, Yasuhiro Tokura*, Yoshiro Hirayama*‡ & Seigo Tarucha*§‖

* *NTT Basic Research Laboratories, NTT Corporation, 3-1 Morinosato-Wakamiya, Atsugi, 243-0198, Japan*
† *Institute for Microstructural Sciences M23A, National Research Council of Canada, Ottawa, Ontario K1A 0R6, Canada*
‡ *CREST Interacting Carrier Electron Project, 4-1-8 Honmachi, Kawaguchi, 331-0012, Japan*
§ *University of Tokyo, Bunkyo-ku, Tokyo, 113-0033, Japan*
‖ *ERATO Mesoscopic Correlation Project, 3-1 Morinosato-Wakamiya, Atsugi, 243-0198, Japan*

The strength of radiative transitions in atoms is governed by selection rules that depend on the occupation of atomic orbitals with electrons[1]. Experiments have shown[2–5] similar electron occupation of the quantized energy levels in semiconductor quantum dots—often described as artificial atoms. But unlike real atoms, the confinement potential of quantum dots is anisotropic, and the electrons can easily couple with phonons of the material[6]. Here we report electrical pump-and-probe experiments that probe the allowed and 'forbidden' transitions between energy levels under phonon emission in quantum dots with one or two electrons (artificial hydrogen and helium atoms). The forbidden transitions are in fact allowed by higher-order processes where electrons flip their spin. We find that the relaxation time is about 200 μs for forbidden transitions, 4 to 5 orders of magnitude longer than for allowed transitions. This indicates that the spin degree of freedom is well separated from the orbital degree of freedom, and that the total spin in the quantum dots is an excellent quantum number. This is an encouraging result for potential applications of quantum dots as basic entities for spin-based quantum information storage.

The quantum dot (QD) that we study is located in a circular pillar (diameter 0.5 μm) fabricated from an AlGaAs/InGaAs heterostructure (Fig. 1a, b and ref. 4). Electrons are confined in an $In_{0.05}Ga_{0.95}As$ quantum well (thickness $a = 12$ nm) in the vertical (z) direction, and approximately by two orthogonal two-dimensional harmonic potentials in the lateral (x and y) direction (corresponding confinement energies, $\hbar\omega_x \approx 2.5$ meV and $\hbar\omega_y \approx 5.5$ meV, where ħ is Planck's constant divided by 2π)[7,8]. As our QD does not have circular symmetry, orbital degeneracy is lifted even at zero magnetic field, and only a twofold spin degeneracy is expected. This non-circularity does not much affect our discussion, and we still use 1s and 2p to label the orbitals for convenience (Fig. 1c).

First we investigate the $N = 1$ QD (artificial hydrogen), in which a single electron occupies the 1s orbital (the ground state) or the 2p orbital (the first excited state). The energy spectrum of these states can be obtained by tunnelling spectroscopy, in which a peak in the derivative of the (source–drain) current with respect to the gate voltage, dI_{sd}/dV_g, appears each time an empty dot state enters the transport window[5]. A colour plot of dI_{sd}/dV_g versus V_g traces taken as a function of magnetic field (B) applied in the z direction is shown in Fig. 1c. The peak spacing within a stripe can be related to the energy spacings between corresponding states. The energy spacing between the 1s and 2p states, ε_{1s-2p}, of the $N = 1$ QD deduced from the first current stripe is plotted in Fig. 2e.

We now focus on the energy relaxation from the 2p state to the 1s state in the $N = 1$ QD, which changes the electron's orbital momentum but preserves the spin. Electrical pump-and-probe experiments are performed by applying a time-dependent gate voltage, $V_g(t)$, which switches between V_l and V_h (Fig. 2a). Experimental details are given in refs 9 and 10. First, the $N = 0$ QD is prepared during the low-phase of the pulse ($V_g = V_l$; Fig. 2b). The period $t_l = 100$–200 ns, is made long enough to ensure that both the 1s and 2p states are empty. When the pulse is switched on ($V_g = V_h$; Fig. 2c), such that only the 2p state is located in the transport window, an electron can be injected into that state from the source (pump) with a time constant $\Gamma_s^{-1} \approx 3$ ns. The electron can only escape to the drain (probe) more slowly, with a time constant $\Gamma_d^{-1} \approx 100$ ns. However, this escape process can be interrupted by the relaxation into the 1s ground state. Thus, the current contains information about the relaxation lifetime, τ_{1s-2p}. We measure the averaged direct current, I_p, under the application of the pulse train. Figure 2d shows how this current changes with the pulse length, t_h. I_p is then converted into an average number of tunnelling electrons per pulse, $\langle n_t \rangle = I_p(t_h + t_l)/e$ (e is the elementary charge). From a detailed analysis of the rate equations including all possible tunnelling processes, we find $\langle n_t \rangle \approx \Gamma_d \tau_{1s-2p}[1 - \exp(-t_h/\tau_{1s-2p})]$ under the condition $\Gamma_s^{-1} \lesssim \tau_{1s-2p} < \Gamma_d^{-1}$, required for the relaxation time measurement[9]. We made sure that this condition was satisfied in all measurements for the $N = 1$ QD. The relaxation time thus estimated from the rise time of $\langle n_t \rangle$ is $\tau_{1s-2p} \approx 10$ ns for the case in Fig. 2d. The small saturation value of $\langle n_t \rangle (\sim 0.02)$ indicates very efficient relaxation.

Our observations for the $N = 1$ QD are consistent with momentum relaxation dominated by spontaneous emission of acoustic phonons at low temperature[6]. Because of the discrete energy of the states, relaxation involves emission of a phonon of energy ε_{1s-2p} (with corresponding wavelength λ_{1s-2p}). In our experiment, ε_{1s-2p}, and hence λ_{1s-2p}, vary with B (Fig. 2e, f). Note also that the characteristic sizes l_x and l_y for the lateral dimensions of the QD decrease with increasing B. The strength of the electron–phonon interaction is expected to be suppressed for values of λ_{1s-2p} that are

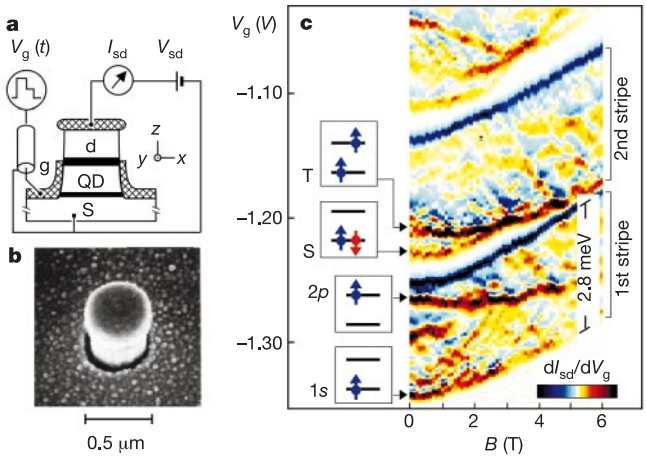

Figure 1 Artificial hydrogen and helium atoms. **a**, Schematic set-up for pulse measurements on the vertical quantum dot (QD). The $In_{0.05}Ga_{0.95}As$ QD is connected to source (s) and drain (d) electrodes made of Si-doped GaAs by asymmetric $Al_{0.22}Ga_{0.78}As$ tunnelling barriers (lower barrier, 7 nm thick; upper barrier, 8.5 nm thick). The tunnelling rates through the barriers, $\Gamma_s \approx (3\,\text{ns})^{-1}$ and $\Gamma_d \approx (100\,\text{ns})^{-1}$, are obtained by separate measurements. The surrounding gate electrode (g) is connected to a pulse generator, which produces a gate voltage, $V_g(t)$, of rectangular or double-step shape. The measurements are performed in a dilution refrigerator at a temperature, T, of ~100 mK, unless otherwise stated, in a magnetic field $B = 0$–5 T applied parallel to the z direction. **b**, Scanning electron micrograph of a control device. **c**, dI_{sd}/dV_g for the $N = 1$ and 2 QD taken with a large source–drain voltage ($V_{sd} = 2.8$ mV). The first (second) stripe gives information about the $N = 1$ (2) QD. The peaks indicated by the arrows show the B-field evolution of the ground state (lowest edge of each stripe) and the first excited state. The relevant 1- and 2- electron configurations are also shown, in which the lower (upper) horizontal line represents the 1s (2p) orbital.

smaller than the characteristic size of the QD (phonon bottleneck effect[11]). Therefore, the B dependence of τ_{1s-2p} in Fig. 2g is because the phonon emission is suppressed (that is, τ_{1s-2p} increases) with decreasing B when λ_{1s-2p} becomes shorter than a, l_x and l_y.

In order to be quantitative, we calculate the phonon emission rate from Fermi's golden rule including both deformation and piezoelectric coupling with standard GaAs material parameters[12,13]. For simplicity, the calculation is done for a circular dot, whose effective confinement energy is $\hbar\omega_{\mathrm{eff}} = \hbar\sqrt{\omega_x\omega_y(1+\omega_c^2/(\omega_x+\omega_y)^2)}$, where ω_c is the cyclotron frequency[7]. As shown by the solid line in Fig. 2g, we find agreement with the data. The difference (by about a factor of 2 or 3) might come from the assumptions about the confinement potential and uncertainties in the material parameters. Thus, the fast energy relaxation in the $N = 1$ QD can be well understood by spontaneous emission of a phonon.

In contrast, the relaxation time is very different for the $N = 2$ QD (artificial helium). At low magnetic fields (see second stripe in Fig. 1c for $B < 2.5$ T), the many-body ground state is a spin singlet (labelled S) with two antiparallel-spin electrons occupying the 1s orbital, while the first excited state is a spin triplet (labelled T) with two parallel-spin electrons, one each occupying the 1s and 2p orbitals[4,5]. Because of Coulomb interactions, the energy spacing between the two states, ε_{S-T} ($\sim$0.6 meV at $B = 0$ T), is smaller than ε_{1s-2p}. Energy relaxation from the first excited state (T) to the ground state (S) not only involves the same change in orbital momentum as that in the $N = 1$ QD, but also requires a spin flip because of Pauli exclusion. A simple phonon-emission transition from the triplet to the singlet is forbidden by spin conservation.

We now investigate to what degree this transition is 'forbidden'. The simple rectangular pulse technique used for the $N = 1$ QD is not useful for this $N = 2$ QD transition, because the relaxation lifetime, τ_{S-T}, is always beyond the measurable range ($\tau_{S-T} > \Gamma_d^{-1} \approx 100$ ns)[9]. Instead, we subject the QD to a double-step voltage pulse, in which V_g is switched between three voltages, V_l, V_h and V_m (Fig. 3a). First, when $V_g = V_l$ (Fig. 3b), the $N = 1$ QD is prepared during a sufficiently long period, $t_l = 100$ ns. When V_g is suddenly increased to V_h (Fig. 3c), an electron can enter to create the $N = 2$ triplet state within the interval $\sim \Gamma_s^{-1} = 3$–7 ns. $V_g = V_h$ for the duration $t_h = 100$ ns–100 μs, which is much longer than Γ_s^{-1}. The triplet may experience a relaxation process during this time. When V_g is changed to V_m (Fig. 3d), an electron in the triplet state can tunnel out to the drain, if the triplet state has not yet

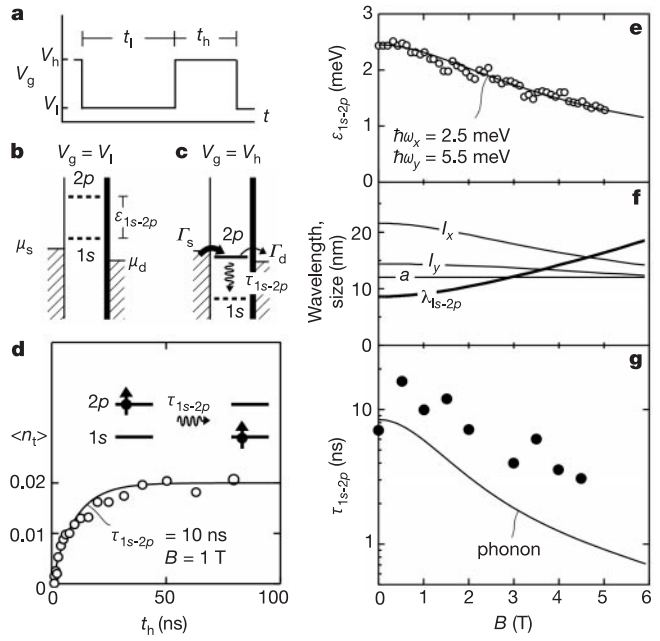

Figure 2 Relaxation time of a one-electron QD (artificial hydrogen atom). **a**, Pulse waveform used for the electrical pump-and-probe experiment (l, low; h, high). **b** and **c**, Schematic energy diagrams along the z direction showing low and high pulse situations. The thick and thin vertical lines denote the asymmetric tunnelling barriers. States in the electrodes are filled up to the Fermi energies, μ_s for the source and μ_d for the drain. The source–drain voltage, V_{sd}, opens a small transport window $eV_{sd} = \mu_s - \mu_d \approx 0.1$ meV. Solid and dashed horizontal lines denote filled and empty single-particle states, respectively. When $V_g = V_l$ (**b**), the 1s and 2p states are located above μ_s and μ_d. When $V_g = V_h$ (**c**), only the 2p state is located in the transport window. The 2p state is pumped from the source at a tunnelling rate, $\Gamma_s \approx (3\,\mathrm{ns})^{-1}$, and probed at a slower rate, $\Gamma_d \approx (100\,\mathrm{ns})^{-1}$. The current measures the momentum relaxation time of the 2p state, τ_{1s-2p}. **d**, The average number of tunnelling electrons per pulse, $\langle n_t \rangle$, measured at 1 T. The relaxation time, $\tau_{1s-2p} = 10$ ns, is obtained from the exponential curve (solid line) fitted to the data. The inset shows the electron configuration before and after relaxation. **e**–**g**, Magnetic field (B) dependence of **e**, the energy spacing between the 2p excited state and the 1s ground state, ε_{1s-2p}, **f**, the longitudinal acoustic photon wavelength, λ_{1s-2p}, and characteristic sizes of the QD (a, l_x and l_y), and **g**, the energy relaxation time, τ_{1s-2p}. The solid line in **e** is a fitted curve with elliptic confinement energies, $\hbar\omega_x \approx 2.5$ meV and $\hbar\omega_y \approx 5.5$ meV. In **f**, λ_{1s-2p} is calculated for the phonon at energy ε_{1s-2p} using a GaAs sound velocity of 5,100 m s^{-1}. The characteristic lateral size in the x/y direction is given by $l_{x/y} = \sqrt{\hbar/m^*}(\omega_{x/y}^2 + \omega_c^2/4)^{-1/4}$, where m^* is the effective mass. The solid line in **g** is calculated for spontaneous emission of an acoustic phonon.

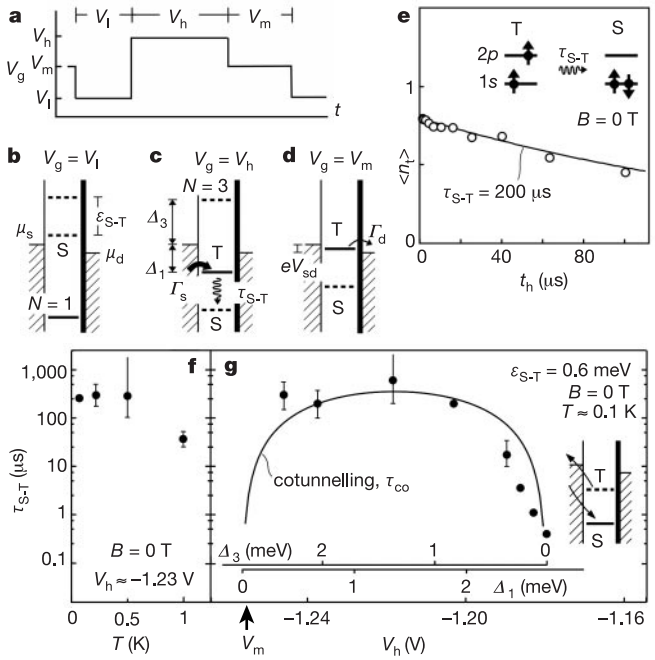

Figure 3 Relaxation time of a two-electron QD (artificial helium atom). **a**, Double-step pulse waveform to measure extremely long relaxation times. **b**–**d**, Schematic energy diagrams showing low, high and intermediate pulse situations. Solid and dashed horizontal lines denote filled and empty many-body states, respectively. $\mu_s - \mu_d \approx 0.1$ meV. When $V_g = V_l$ (**b**), the spin-singlet ground state S and the spin-triplet first excited state T are located above μ_s and μ_d. The system will always become the $N = 1$ QD after a sufficiently long period, $t_l = 100$ ns. When $V_g = V_h$ (**c**), the QD can be excited to the triplet state within $\Gamma_s^{-1} \approx 7$ ns. The triplet state can then relax to the singlet state during the period, $t_h = 0.1$–100 μs. When $V_g = V_m$ (**d**), the triplet state is probed by allowing an electron to tunnel into the drain. This period is fixed at $t_m = 300$ ns. **e**, Average number of tunnelling electrons per pulse, $\langle n_t \rangle$ at 0 T. The relaxation time, $\tau_{S-T} = 200$ μs, is obtained from the exponential decay (solid line). Inset, electron configuration before and after relaxation. **f**, Temperature (T) dependence of the relaxation time τ_{S-T} at 0 T. **g**, The gate voltage (V_h) dependence of τ_{S-T}. V_h is also converted into Δ_1 and Δ_3 energy scales. Δ_1 and Δ_3 are indicated in **c**. The solid line is calculated for cotunnelling processes. Inset, diagram of these inelastic cotunnelling processes.

relaxed to the singlet state. We set the period, $t_m = 300$ ns, to be longer than Γ_d^{-1} so we can read out the signal. We repeatedly apply the double-step pulse (effectively $\sim 10^7$ times) to obtain a reliable current I_p, and evaluate the average number of tunnelling electrons $\langle n_t \rangle = I_p(t_l + t_h + t_m)/e$. As the current measures the unrelaxed electron number, $\langle n_t \rangle = A \exp(-t_h/\tau_{S-T})$ for the condition $\Gamma_s^{-1} \lesssim \tau_{S-T}$ (no upper limit in principle), where $A \approx 1$ is approximately the ratio of Γ_s^{-1} for the triplet to that for the singlet. Figure 3e shows a typical measurement of $\langle n_t \rangle$ at 0 T, indicating a relaxation time of $\tau_{S-T} \approx 200\,\mu$s. This relaxation time is 4 to 5 orders of magnitude longer than that observed in the $N = 1$ QD.

Looking at the properties of τ_{S-T}, we find no clear B dependence (always longer than 100 μs), at least for ε_{S-T} between 0.6 meV at $B = 0$ T and 0.24 meV at $B = 2$ T (not shown). We also investigate the temperature dependence (Fig. 3f), but not clear change is observed up to 0.5 K. τ_{S-T} decreases above 0.5 K, where thermal excitation from the QD to the electrodes becomes important. On the other hand, we do find that τ_{S-T} strongly depends on the high gate-pulse voltage V_h, during which relaxation takes place (Fig. 3g). Although V_h is deep in the $N = 2$ Coulomb blockade region ($-1.27\,V < V_h < -1.16\,V$), τ_{S-T} decreases rapidly at $V_h \approx -1.18\,V$. This V_h dependence implies a strong influence of the electrodes. Even though the Coulomb blockade is robust in the suppression of transport, higher-order tunnelling processes can contribute to the relaxation. An electron in the dot can be replaced with an electron of opposite spin from the electrodes (see Fig. 3g inset). This results in energy relaxation in the QD, and the electrode gains the same energy. This inelastic cotunnelling rate, τ_{co}^{-1}, is estimated by considering second-order tunnelling processes[14–16]. For the relaxation mechanisms considered here, the $N = 2$ QD can relax virtually through $N = 1$ or $N = 3$ intermediate states. Note that this process does not cause a net current, even at a finite voltage of $e|V_{sd}| < \varepsilon_{S-T}$ (ref. 17). Assuming $V_{sd} = 0$ V and zero temperature for simplicity, we obtain $\tau_{co}^{-1} = \varepsilon_{S-T}(\hbar\Gamma_s + \hbar\Gamma_d)^2(\Delta_1^{-1} + \Delta_3^{-1})^2/h$. Here, Δ_1 and Δ_3 are respectively the energies required to excite the initial $N = 2$ triplet state to the $N = 1$ and 3 intermediate states (Fig. 3c). We can extract Δ_1 and Δ_3 from V_h, and the values are shown in Fig. 3g. The solid line shows τ_{co}, the relaxation time due to cotunnelling, calculated with experimentally deduced parameters ($\varepsilon_{S-T} = 0.6$ meV, and $(\Gamma_s + \Gamma_d)^{-1} = 7$ ns). The observed relaxation time can be well understood by inelastic cotunnelling.

Our observations for $N = 1$ and 2 QDs can be compared with real atoms[1]. The transition from the $2p$ state to the $1s$ state in atomic hydrogen is allowed by photon emission, whereas that in artificial hydrogen is allowed by phonon emission. The transition from the spin-triplet state to the spin-singlet state is forbidden by conservation of the total spin for both atomic helium and artificial helium. The difference between the allowed and forbidden transitions leads to more than 11 orders of magnitude difference in the relaxation times for real hydrogen and helium atoms. Our observation of 4 to 5 orders of magnitude difference in artificial atoms is not as high, but is still surprisingly large. (Note that this difference would become larger if the cotunnelling could be suppressed by using thicker tunnelling barriers.) Very importantly, the large difference between τ_{1s-2p} and τ_{S-T} originates from the fact that other effects, such as spin-orbit and hyperfine interactions[18,19], must have only a weak effect on the breaking of the 'forbidden' symmetries. We now discuss how small these hidden contributions are by focusing on spin–orbit interactions.

Spin–orbit interactions are predicted to give the dominant contribution to spin relaxation in GaAs QD systems[19], although this is still an extremely small effect. For simplicity, we consider the spin–orbit interaction energy, Δ_{so}, only for coupling between the $1s$ and $2p$ orbitals, but include all effects that mix spin and orbital degrees of freedom. Simple perturbation theory[20] predicts that the relaxation time from the triplet to the singlet is given by $\tau_{S-T,so} \approx (\varepsilon_{S-T}/\Delta_{so})^2 \tau_{phonon}(\varepsilon_{S-T})$. Here, $\tau_{phonon}^{-1}(\varepsilon_{S-T})$ is the phonon emission rate at the phonon energy, ε_{S-T}, and we know that τ_{phonon} is well accounted for by the electron–phonon interaction. Therefore, we can deduce an upper bound of $\Delta_{so} < 4\,\mu$eV from our observations ($\tau_{S-T} > 200\,\mu$s). This value is close to the spin splitting energy ($\sim 2.5\,\mu$eV) observed in a GaAs two-dimensional electron gas system[21].

Our experiments indicate that the spin degree of freedom in QDs is well separated from the orbital degree of freedom. This is particularly attractive for applications to spin memories and spin quantum bits (qubits)[22–24]. For a simple scheme involving just a single-electron spin in a magnetic field, the spin–orbit interactions can affect the energy relaxation time (T_1) of a spin qubit. We estimate the dominant contribution, $T_{1,so}$, using a perturbative approach: $T_{1,so} \approx (\varepsilon_{1s-2p}/\Delta_{so})^2 \tau_{phonon}(\varepsilon_Z)$. As $\Delta_{so} < 4\,\mu eV$, this yields $T_{1,so} > 1$ ms for a Zeeman splitting (unresolved in our measurement) $\varepsilon_Z \approx 0.1$ meV and $\varepsilon_{1s-2p} \approx 1.2$ meV at $B \approx 5$ T ($T_{1,so} > 100\,\mu$s at B ≈ 9 T). This $T_{1,so}$ is thus comparable to that obtained by electron spin resonance for donor states in GaAs (ref. 25), and is much longer than the time required for typical one- and two-qubit operations[26]. Note that small spin–orbit interactions are also desirable with respect to the dephasing time (T_2) of a spin qubit[27]. Our results therefore encourage further research on the use of the spin degree of freedom in QDs. □

Received 2 May; accepted 5 July 2002; doi:10.1038/nature00976.

1. Bethe, H. A. & Salpeter, E. E. *Quantum Mechanics of One- and Two-Electron Atoms* (Springer, Berlin, 1957).
2. Kouwenhoven, L. P., *et al.* in *Mesoscopic Electron Transport* NATO ASI series E 345 (eds Sohn, L. L., Kouwenhoven, L. P. & Schön, G.) 105–214 (Kluwer, Dordrecht, 1997).
3. Ashoori, R. C. *et al.* Single-electron capacitance spectroscopy of discrete quantum levels. *Phys. Rev. Lett.* **68,** 3088–3091 (1992).
4. Tarucha, S., Austing, D. G., Honda, T., van der Hage, R. J. & Kouwenhoven, L. P. Shell filling and spin effects in a few electron quantum dot. *Phys. Rev. Lett.* **77,** 3613–3616 (1996).
5. Kouwenhoven, L. P. *et al.* Excitation spectra of circular, few-electron quantum dots. *Science* **278,** 1788–1792 (1997).
6. Fujisawa, T. *et al.* Spontaneous emission spectrum in double quantum dot devices. *Science* **282,** 932–935 (1998).
7. Tokura, Y., Sasaki, S., Austing, D. G. & Tarucha, S. Excitation spectra and exchange interactions in circular and elliptical quantum dots. *Physica B* **298,** 260–264 (2001).
8. Matagne, P., Leburton, J. P., Austing, D. G. & Tarucha, S. Shell charging and spin-filling sequences in realistic vertical quantum dots. *Phys. Rev. B* **65,** 085325 (2002).
9. Fujisawa, T., Tokura, Y. & Hirayama, Y. Transient current spectroscopy of a quantum dot in the Coulomb blockade regime. *Phys. Rev. B* **63,** 081304 (2001).
10. Fujisawa, T., Austing, D. G., Tokura, Y., Hirayama, Y. & Tarucha, S. Non-equilibrium transport through a vertical quantum dot in the absence of spin-flip energy relaxation. *Phys. Rev. Lett.* **88,** 236802 (2002).
11. Benisty, H., Sotomayer-Torres, C. M. & Weisbuch, C. Intrinsic mechanism for the poor luminescence properties of quantum-box systems. *Phys. Rev. B* **44,** 10945–10948 (1991).
12. Seeger, K. *Semiconductor Physics: An Introduction* 153–213 (Springer, Berlin, 1985).
13. Bockelmann, U. Phonon scattering between zero-dimensional electronic states: Spatial versus Landau quantization. *Phys. Rev. B* **50,** 17271–17279 (1994).
14. Averin, D. V. & Nazarov, Yu. V. in *Single Charge Tunneling: Coulomb Blockade Phenomena in Nanostructures* (eds Grabert, H. & Devoret, M. H.) 217–247 (Plenum and NATO Scientific Affairs Division, New York, 1992).
15. Eto, M. Electronic states and transport phenomena in quantum dot systems. *Jpn J. Appl. Phys. 1* **40,** 1929–1935 (2001).
16. Sukhorukov, E. V., Burkard, G., Loss, D.. *Phys. Rev. B* **63,** 125315 (2001).
17. De Franceschi, S. *et al.* Electron cotunneling in a semiconductor quantum dot. *Phys. Rev. Lett.* **86,** 878–881 (2001).
18. Pikus, G. E. & Titkov, A. N. in *Optical Orientation* (eds Meier, F. & Zakharchenya, B. P.) 73–131 (Elsevier, Amsterdam, 1984).
19. Khaetskii, A. V. & Nazarov, Yu. V. Spin relaxation in semiconductor quantum dots. *Phys. Rev. B* **61,** 12639–12642 (2000).
20. Halperin, W. P. Quantum size effects in metal particles. *Rev. Mod. Phys.* **58,** 533–606 (1986).
21. Bychkov, Yu. A. & Rashba, E. I. Properties of a 2D electron gas with lifted spectral degeneracy. *JETP Lett.* **39,** 78–81 (1984).
22. Loss, D. & DiVincenzo, D. P. Quantum computation with quantum dots. *Phys. Rev. A* **57,** 120–126 (1998).
23. Recher, P., Sukhorukov, E. V. & Loss, D. Quantum dot as spin filter and spin memory. *Phys. Rev. Lett.* **85,** 1962–1965 (2000).
24. Ciorga, M. *et al.* Readout of a single electron spin based quantum bit by current detection. *Physica E* **11,** 35–40 (2001).
25. Seck, M., Potemski, M. & Wyder, P. High-field spin resonance of weakly bound electrons in GaAs. *Phys. Rev. B* **56,** 7422–7427 (1997).
26. Gupta, J. A., Knobel, R., Samarth, N. & Awschalom, D. D. Ultrafast manipulation of electron spin coherence. *Science* **292,** 2458–2461 (2001).
27. Kavokin, K. V. Anisotropic exchange interaction of localized conduction-band electrons in semiconductors. *Phys. Rev. B* **64,** 075305 (2001).

Acknowledgements

We thank G. E. W. Bauer, T. Honda, T. Inoshita, A. V. Khaetskii and L. P. Kouwenhoven for discussions and help.

Competing interests statement

The authors declare that they have no competing financial interests.

Correspondence and requests for materials should be addressed to T.F. (e-mail: fujisawa@will.brl.ntt.co.jp).

Forward scattering due to slow-down of the intermediate in the H + HD → D + H_2 reaction

Steven A. Harich*, Dongxu Dai*†, Chia C. Wang*‡, Xueming Yang*†§, Sheng Der Chao‖¶ & Rex T. Skodje‖¶

* *Institute of Atomic and Molecular Sciences, Academia Sinica, Taipei, Taiwan*
† *Dalian Institute of Chemical Physics, Chinese Academy of Sciences, Dalian, China*
‡ *Department of Chemistry, National Taiwan University, Taipei, Taiwan*
§ *Department of Chemistry, National Tsing Hua University, Hsinchu, Taiwan*
‖ *Institute of Molecular Science, Myodaiji, Okazaki 444-8585, Japan*
¶ *Department of Chemistry and Biochemistry, University of Colorado, Boulder, Colorado 80309, USA*

Quantum dynamical processes near the energy barrier that separates reactants from products influence the detailed mechanism by which elementary chemical reactions occur. In fact, these processes can change the product scattering behaviour from that expected from simple collision considerations, as seen in the two classical reactions F + H_2 → HF + H and H + H_2 → H_2 + H and their isotopic variants. In the case of the F + HD reaction, the role of a quantized trapped Feshbach resonance state had been directly determined[1], confirming previous conclusions[2] that Feshbach resonances cause state-specific forward scattering of product molecules. Forward scattering has also been observed in the H + D_2 → HD + D reaction[3,4] and attributed to a time-delayed mechanism[3,5–7]. But despite extensive experimental[8–12] and theoretical[13–18] investigations, the details of the mechanism remain unclear. Here we present crossed-beam scattering experiments and quantum calculations on the H + HD → H_2 + D reaction. We find that the motion of the system along the reaction coordinate slows down as it approaches the top of the reaction barrier, thereby allowing vibrations perpendicular to the reaction coordinate and forward scattering. The reaction thus proceeds, as previously suggested[7], through a well-defined 'quantized bottleneck state' different from the trapped Feshbach resonance states observed before.

In this work, we studied the H + HD → H_2 + D reaction experimentally using the H(D)-atom Rydberg time-of-flight (HRTOF) technique, developed in refs 12 and 19. We measured time-of-flight (TOF) spectra of the D-atom products at different laboratory scattering angles at the collisional energy of 1.200 eV. The TOF spectra measured are then converted to the centre-of-mass product translational energy distributions. Different H_2-product rovibrational states can be resolved clearly in this experiment. From these distributions, relative quantum state-specific differential cross-sections (DCS) are obtained. On the basis of this measured data, a full three-dimensional (3D) product contour plot is constructed and shown in Fig. 1. One of the most interesting observations is the forward scattering peak seen in Fig. 1, similar to the forward scattering observed in the H + D_2 reaction[3–5] at higher collisional energies. The characteristics of the forward scattering H_2 products are unique. First, it is clear that the forward scattering H_2-products are significantly colder rotationally, with mainly $H_2(j' = 1)$ populated, than the backwards and sideways scattering products. Second, the angle range of the observed forward scattering peak is extremely narrow. Experimental characteristics of the forward scattering peak including the rotational distribution and the angular width can be readily reproduced by the quantum calculations. However, to assign the forward peak to specific dynamical behaviour requires further theoretical analysis.

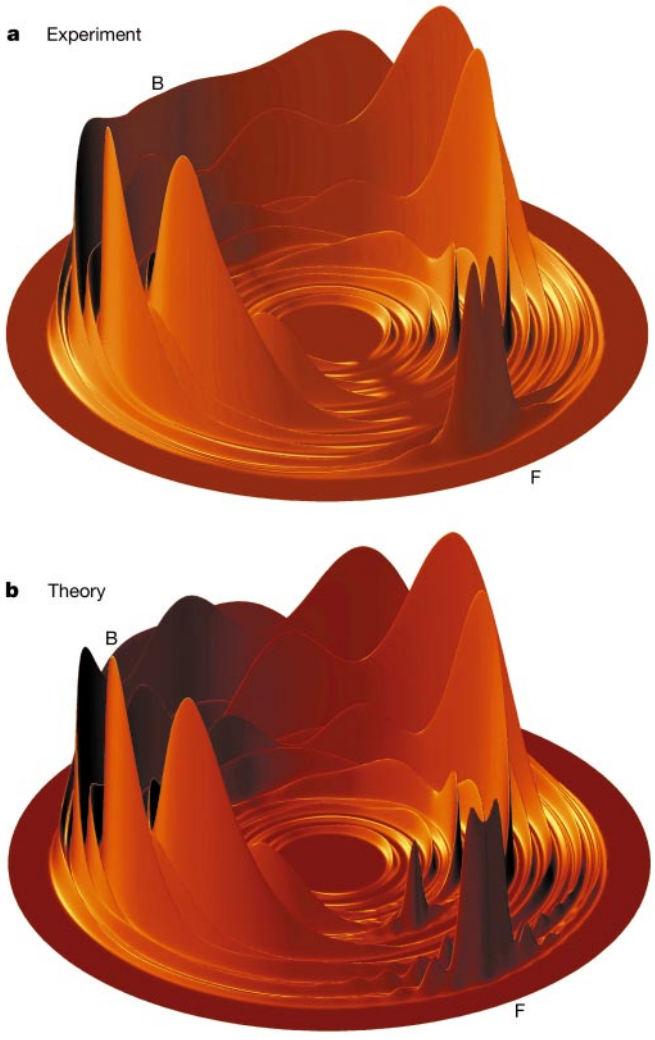

Figure 1 Three-dimensional product contour plots as a function of product velocity. Shown are product contour plots versus product velocity in the centre-of-mass frame obtained experimentally (**a**) and theoretically (**b**). Experimentally, time-of-flight spectra of the D-atom product were measured at every 5 degrees and then converted into the translational energy distribution in the centre-of-mass frame. From these translational energy distributions, the angular distributions of all H_2-product quantum states can be determined. The experimental 3D product contour plot (**a**) is obtained from fitting smoothly the experimental angular distributions of all product (H_2) quantum states using a multi-order polynomial function. Theoretically, the *S*-matrix for H + HD was calculated using quantum-reactive scattering methods described previously[17,18], on the BKMP2 PES[20]. Differential cross-sections (DCS) at different centre-of-mass angles were computed from the *S*-matrix. The theoretical 3D product contour plot is constructed from these calculated DCS. The forward-scattering direction ($\theta = 0°$) is denoted F and the backward-scattering direction is denoted B. The height of the peaks represents the magnitude of DCS, while the radius from the centre represents the product translational energy, E_T.